Chapter 3

Optimal Scheduling of PHEVs and D-BESSs in the Presence of DGs in Distribution System

3.1 Introduction

The emergence of active distribution system with the integration of prosumers and distributed energy resources (DERs) has been discussed in the first chapter. Large and uncoordinated penetration of Electric Vehicles (EVs) in the distribution system can adversely affect system performance measures such as loading, voltage deviations, network losses, and power quality issues. Coordinated charging is one of the solutions to address these problems. Plug-in Hybrid Electric Vehicles (PHEVs) are equipped with large battery capacities, thereby increasing energy storage capacity in the system. The Vehicle-to-Grid (V2G) mode operation of PHEVs can provide backup reserve support to the system, which can also be used to minimize system peak demands. The increased level of renewable energy generation in the system reduces CO_2 emissions and energy losses. Optimization of cost and load flattening for a distribution network is attempted in this chapter. The objective function is described in terms of energy cost, CO_2 emissions, real power losses, and load flattening. The solution is envisaged in terms of hourly scheduling of DGs, Distributed Battery Energy Storage Systems (D-BESSs), and PHEVs. Further, an investigation into reformulation of the cost of energy is carried out to eliminate the solutions involving excessive charging and discharging of batteries in the system (i.e.,

BESSs/D-BESSs and PHEVs).

It is demonstrated that simultaneous optimization of cost, CO_2 emissions, real power losses, and load flattening cannot be effectively solved as a weighted sum of objective functions. An appropriate weighted sum formulation needs Pareto Front consideration for determining the weights, and there are situations where the weighted sum cannot be judiciously employed for formulating the objective function. In most of the cases, the linear weighted sum method is inadequate to represent the non-extreme efficient solutions. The weighted sum method is strongly affected by the convexity of the problem and scaling of objective functions.

The ε-constraint method is able to generate the exact Pareto optimal of any multi-objective optimization problem unaffected by the convexity of the problem [124]. In this chapter, an ε-constraint method is applied to obtain the optimal scheduling to achieve cost optimization, load flattening, and minimization of CO_2 emissions from the Distribution Utility (DU) point of view. A variation in the optimization problem is attempted by introducing a sub-problem of decentralized optimization of the energy cost of PHEVs and D-BESSs retaining the constraints of the main problem. This variation allows the practical consideration of allowing the aggregators to optimize the resources in their favor. It is observed that the combination of the scheduling of DGs, BESSs/D-BESSs, and G2V/V2G can successfully be used to significantly reduce the system peak demand along with system cost, losses, and CO_2 emissions.

3.2 Problem formulation

3.2.1 Objective functions

The objective function (F) consists of four components corresponding to cost of energy (f_1), CO_2 emission (f_2), real power losses (f_3), and load flattening (f_4). Thus, the objective function can be written as

$$\min \mathrm{F}(f_1, f_2, f_3, f_4). \tag{3.1}$$

The component f_1, f_2, f_3, and f_4 can be explained as follows.

Energy Cost (f_1)

The cost of energy (f_1) is calculated as the sum of the cost of energy import from the grid (C_G), cost of energy from DGs (C_{DG}), curtailment cost of DGs (C_{DGC}), cost of D-BESSs (C_{BESS}) and PHEVs (C_{EV}). Thus, f_1 can be written as

$$f_1 = C_G + C_{DG} + C_{DGC} + C_{EV} + C_{BESS}, \tag{3.2}$$

where,

$$C_G = \sum_{t=1}^{T} \Bigg[\Bigg(\sum_{k=1}^{N_{bus}} \Bigg(P_t^{L,k} + \sum_{b=1}^{N_{bess}} P_t^{c,b,k} + \sum_{ev=1}^{N_{ev}} P_t^{c,ev,k} - \sum_{b=1}^{N_{bess}} P_t^{d,b,k} - \sum_{ev=1}^{N_{ev}} P_t^{d,ev,k} \Bigg) - \sum_{dg=1}^{N_{dg}} P_t^{dg} + \sum_{l=1}^{N_{branch}} P_t^{loss,l} \Bigg) \rho_t^g \Bigg], \tag{3.3}$$

$$C_{DG} = \sum_{t=1}^{T} \sum_{dg=1}^{N_{dg}} P_t^{dg} \rho_t^{dg}, \tag{3.4}$$

and

$$C_{DGC} = \sum_{t=1}^{T} \sum_{dg=1}^{N_{dg}} (P_t^{DGmax,dg} - P_t^{dg}) \rho_t^{cur,dg}. \tag{3.5}$$

C_{EV} consists of both charging and discharging costs and can be described as [75]

$$C_{EV} = \sum_{t=1}^{T} \sum_{k=1}^{N_{bus}} \sum_{ev=1}^{N_{ev}} (P_t^{d,ev,k} \rho_t^d - P_t^{c,ev,k} \rho_t^c). \tag{3.6}$$

Similarly, for D-BESSs, the C_{BESS} can be written as

$$C_{BESS} = \sum_{t=1}^{T} \sum_{k=1}^{N_{bus}} \sum_{b=1}^{N_{bess}} (P_t^{d,b,k} \rho_t^d - P_t^{c,b,k} \rho_t^c). \tag{3.7}$$

Equations (3.6) and (3.7) represent the net cost incurred by the utility as a difference of discharging cost and charging cost of PHEVs and D-BESSs. The charging price $\rho^c \geq \rho^g$ as ρ^c may have some fixed charges, i.e. network and metering costs in addition to ρ^g. ρ^d can be less than or greater than ρ^g. There is not much clarity on ρ^d in literature. It can be seen that the charging of PHEVs i.e. $\sum_{ev=1}^{N_{ev}} P_t^{c,ev,k}$ have been already considered in C_G in Equation (3.3) as part of system load as a positive term, whereas it is considered as a negative term in C_{EV} in Equation (3.6). The total cost when C_G, C_{EV}, and C_{BESS} are added, yields

$$min \Bigg[\sum P_t^c (\rho_t^g - \rho_t^c) + \sum P_t^d (\rho_t^d - \rho_t^g) \Bigg]. \tag{3.8}$$

In Equation (3.8) it is worth noting that the net value of the first term will always be zero or negative and second term varies as the difference between ρ^g and ρ^d. So to minimize the objective function, there is a tendency to maximize charging power, P_t^c, in Equation (3.8) when $\rho^c > \rho^g$, and to maximize discharging power, P_t^d, when $\rho^d < \rho^g$. Thus, this promotes a scheduling, which gives rise to excessive charging and discharging of PHEVs and D-BESSs during certain hours. This phenomena of excessive charging and discharging would be demonstrated in section 3.6. Also, "$-C_{EV}$" is a term which will be added in consumer electricity charge. So the minimization of C_{EV} will reflect as maximization of "$-C_{EV}$" from a consumer point of view. Thus, charging term should be eliminated from Equation (3.6) for optimization purposes as it nullifies its own effect. Consequently, Equation (3.6) is modified as given in Equation (3.9). However, the cost of energy to the utility should be based on Equation (3.6).

$$C_{EV}^{'} = \sum_{t=1}^{T} \sum_{k=1}^{N_{bus}} \sum_{ev=1}^{N_{ev}} P_t^{d,ev,k} \rho_t^d. \tag{3.9}$$

Similarly, for D-BESSs, the $C_{BESS}^{'}$ can be written as

$$C_{BESS}^{'} = \sum_{t=1}^{T} \sum_{k=1}^{N_{bus}} \sum_{b=1}^{N_{bess}} P_t^{d,b,k} \rho_t^d. \tag{3.10}$$

Thus, the modified objective function ($f_1^{'}$) can be written as

$$f_1^{'} = C_G + C_{DG} + C_{DGC} + C_{EV}^{'} + C_{BESS}^{'}. \tag{3.11}$$

The effectiveness of the proposed objective function will be demonstrated numerically in section 3.6.

CO_2 Emission (f_2)

The term f_2 related to CO_2 emission can be expressed as

$$f_2 = E_{CO_2\_G} + E_{CO_2\_DG} - E_{CO_2\_conv\_veh}, \tag{3.12}$$

where, $E_{CO_2\_G}$ is CO_2 emission due to conventional thermal power plant and can be written as

$$E_{CO_2\_G} = \sum_{t=1}^{T} K_{CO_2\_G} P_t^g, \tag{3.13}$$

$E_{CO_2\_DG}$ is CO_2 emission due to Fuel Cell (FC) based DGs and can be written as

$$E_{CO_2\_DG} = \sum_{t=1}^{T} \sum_{dg=1}^{N_{dg}} K_{CO_2\_DG} P_t^{dg}, \tag{3.14}$$

and $E_{CO_2\_conv\_veh}$ is CO_2 emission due to conventional combustion engine vehicles and can be written as

$$E_{CO_2\_conv\_veh} = \sum_{ev=1}^{N_{ev}} K_{CO_2\_conv\_veh} D_{km}^{ev}. \tag{3.15}$$

This component is treated as negative in Equation (3.12), as conventional vehicles are replaced by EVs.

Real Power Losses (f_3)

The term f_3 related to real power losses in the system can be expressed as

$$f_3 = \sum_{t=1}^{T} \sum_{l=1}^{N_{branch}} P_t^{loss,l}. \tag{3.16}$$

Load Flattening (f_4)

The term f_4 related to load flattening can be defined as

$$f_4 = \sum_{t=1}^{T} \left(P_t^g - \bar{P}^g \right)^2, \tag{3.17}$$

where, P_t^g is the total demand at the Point of Common Coupling (PCC) that is supplied by the grid and is expressed as

$$P_t^g = \sum_{k=1}^{N_{bus}} \Bigg(P_t^{L,k} + \sum_{b=1}^{N_{bess}} (P_t^{c,b,k} - P_t^{d,b,k}) + \sum_{ev=1}^{N_{ev}} (P_t^{c,ev,k} - P_t^{d,ev,k}) \Bigg) + \sum_{l=1}^{N_{branch}} P_t^{loss,l} - \sum_{dg=1}^{N_{dg}} P_t^{dg}. \tag{3.18}$$

$\bar{P}^g$ is the average power demand during 24 hours and can be defined as

$$\bar{P}^g = \frac{1}{T} \sum_{t=1}^{T} P_t^g. \tag{3.19}$$

Function f_4 helps to reduce the Peak to Average Ratio (PAR), thereby increasing the load factor, which may further lead to the reduction of peak load prices. Flattening of the load curve ensures reduced reservoir (peak load plants) capacity. Also, a decrease in the

peak of load curve ensures that if any hike occurs in system load due to the variability of RES or PHEVs, then the system has sufficient margins. Also, lowering the PAR allows deferment of investment for system upgrades.

The charging/discharging pattern of PHEVs affects all four objectives as follows.

- Cost (f_1): The unscheduled charging of PHEVs is not beneficial for both the EVs' owner and utility. The unscheduled charging may lead to higher costs if they get charged during high tariff periods.

- CO_2 emissions (f_2): However, the replacement of conventional vehicles by EVs reduces CO_2 emission but if the power demand of EVs is supplied by conventional generation then it will cause high CO_2 emission. Therefore, the effective coordination of RES and EVs demand needed to be investigated.

- Losses (f_3): Uncoordinated charging may lead to higher voltage drop and power losses.

- Load flattening (f_4): The battery storage capacity of EVs/PHEVs can be used to minimize peak demand and fill valleys in distribution systems.

3.2.2 Constraints

The objective function is subjected to the following constraints which must be satisfied during normal operating conditions.

Power balance constraints

Equations (3.20) and (3.21) represent instantaneous active and reactive power balance for the system, respectively.

$$-P_t^{L,k} + P_t^{dg,k} - \sum_{b=1}^{N_{bess}} (P_t^{c,b,k} - P_t^{d,b,k}) - \sum_{ev=1}^{N_{ev}} (P_t^{c,ev,k} - P_t^{d,ev,k}) - \sum_{j=1}^{N_{bus}} V_t^k V_t^j [G^{kj} cos\delta_t^{kj} + B^{kj} sin\delta_t^{kj}] \leq \epsilon. \quad (3.20)$$

In the Equation (3.20), the DG power ($P_t^{dg,k}$), charging & discharging power of D-BESS ($P_t^{c,b,k}$ & $P_t^{d,b,k}$), and charging & discharging power of PHEV ($P_t^{c,ev,k}$ & $P_t^{d,ev,k}$) will be

zero for k^{th} bus if there are no DG, D-BESS and PHEV.

$$-Q_t^{L,k} + \sum_{j=1}^{N_{bus}} V_t^k V_t^j [B^{kj} cos\delta_t^{kj} - G^{kj} sin\delta_t^{kj}] \leq \epsilon. \tag{3.21}$$

It is assumed that DGs, PHEVs, and D-BESSs will not be consume or generate reactive power.

Bus voltage constraint

Equation (3.22) bounds the bus voltage magnitudes within limits.

$$V^{min} \leq V_t^k \leq V^{max}, \tag{3.22}$$

DG power output

Constraint (3.23) imposes the maximum and minimum active power injection limits by DGs.

$$P_t^{DGmin,dg} \leq P_t^{dg} \leq P_t^{DGmax,dg}. \tag{3.23}$$

Battery technical limit for PHEV and BESS

Simultaneous charge and discharge of batteries are constrained as follows.

$$P_t^{c,i} P_t^{d,i} = 0. \tag{3.24}$$

The State-of-Charge (SoC) limits of the battery are constraints as

$$SoC^{min,i} \leq SoC_t^i \leq SoC^{max,i}, \tag{3.25}$$

where, i stands for a battery of either PHEV or D-BESS.

Equation (3.26) indicates the SoC at the next state, t of D-BESS and PHEV based on charging/discharging power and can be defined as

$$SoC_t^i = SoC_{t-1}^i + \frac{100}{BC^i}\left(\eta_c P_t^{c,i} - \frac{P_t^{d,i}}{\eta_d}\right). \tag{3.26}$$

The charging and discharging power of batteries are also constrained according to the maximum charging and discharging rate specified and battery SoC status. The Maximum charging and discharging limits are defined by the constraints (3.27) and (3.28), respectively.

$$\eta_c P_t^{c,i} \leq min\left[P^{cmax,i}, \left(\frac{BC^i}{100}\left(SoC^{max,i} - SoC_{t-1}^i\right)\right)\right], \tag{3.27}$$

and

$$\frac{P_t^{d,i}}{\eta_d} \leq min\left[P^{dmax,i}, \left(\frac{BC^i}{100}\left(SoC_{t-1}^i - SoC^{min,i}\right)\right)\right]. \tag{3.28}$$

Another constraint imposed on D-BESSs is to ensure that net storage used by the utility is equal to zero, over a day. Otherwise, there may be a possibility that D-BESSs are left out at minimum SoC level at the end of the day in an attempt to reduce cost and line losses. This constraint can be written as

$$\sum_{t=1}^{T} \eta_c P_t^{c,i} = \sum_{t=1}^{T} \frac{P_t^{d,i}}{\eta_d}. \tag{3.29}$$

The constraint for PHEVs to get maximum possible SoC at departure time is stated as follows.

$$\Delta T = \begin{cases} (t_{depa} - t_{arri}) & t_{arri} < t_{depa} \\ 24 + (t_{depa} - t_{arri}) & t_{arri} > t_{depa} \end{cases}, \tag{3.30}$$

$$SoC_{t_{depa}}^{ev} = \left[min\left(100, \left(SoC_{t_{arri}}^{ev} + \frac{P^{cmax,ev}}{BC^{ev}}\Delta T \times 100\right)\right)\right]. \tag{3.31}$$

To implement the proposed formulation, the stochastic model of SoC profile of PHEVs is to be developed. The RES-based DGs are considered to be curtailable. The PHEVs are scheduled in such a way that consumer gets the maximum possible level of SoC at departure time. The D-BESSs are scheduled such that SoC level is always maintained greater than 30% for consumer uses during short period power-curtailment. In the present work, a single value of 30% is taken, however, this value can be different for different consumers as per contract.

3.3 Stochastic model of PHEVs

Battery SoC represents the estimated available charge in the battery. Accurate knowledge of SoC is required for scheduling of PHEV in V2G and G2V mode. However, it is difficult to estimate SoC of PHEV during operation. Coulomb counting method is most commonly used for determining the SoC [125].

The mathematical expression of SoC can be given as

$$SoC = \left(1 - \frac{\Gamma\Upsilon}{AER}\right)100, \;\; \Gamma\Upsilon \leq \Gamma_{aer}, \tag{3.32}$$

where Υ is the fraction of the total distance traveled in electric mode and Γ is the total traveled distance and Γ_{aer} is the possible All Electric Range (AER) of a Vehicle.

The energy required to charge the PHEV fully is calculated as

$$E^{ev} = \frac{1 - \frac{SoC_{t_{arri}}}{100}}{\eta_c} BC. \tag{3.33}$$

The relationship between energy required, distance traveled and battery capacity can be explained through the following example. Let a full-size SUV of type PHEV-60 (i.e. PHEV with AER = 60 miles) have a battery capacity of 27.6 kW. If the distance traveled by the vehicle is considered as 50 miles and $\Upsilon = 70\%$, then the $SoC_{t_{arri}}$ is calculated as

$$SoC_{t_{arri}} = (1 - \frac{0.70 \times 50}{60}) \times 100,$$

$$SoC_{t_{arri}} = 41.667\%,$$

and the energy required to charge the PHEV fully is calculated as

$$E^{ev} = \frac{1 - \frac{41.667}{100}}{0.95} \times 27.6 = 16.947kWh.$$

In this work, NHTS-2009 [126] data is used to generate parameters of PHEVs. NHTS-2009 database consists of 1048575 single trips each having 150 attributes such as arrival time, departure time, trip distance, and trip time. The SoC profile of PHEVs are generated by Monte-Carlo simulation. Figure 3.1 shows the distribution of traveled distance, SoC level of vehicles at arrival time, arrival time, and departure time of PHEVs. Table 3.1 shows the parameters [31] considers for generating the data through Monte-Carlo simulation. There are different possible probability distribution functions which may fit the data for Figure 3.1(c) and 3.1(d). However, we have used normal distribution in present work to maintain the consistency with [31].

Table 3.1: PHEVs related parameters

Type of vehicles	1,2,3, and 4
Battery capacity	7.8-27.6 kWh
Arrival time	$\mathcal{N}(\mu = 17.01, \sigma^2 = 10.24)$
Departure time	$\mathcal{N}(\mu = 9.97, \sigma^2 = 4.84)$
Distance traveled	Lognormal($\mu = 3.2$ and $\sigma^2 = 0.81$)
Distribution factor (Υ)	0.5-1

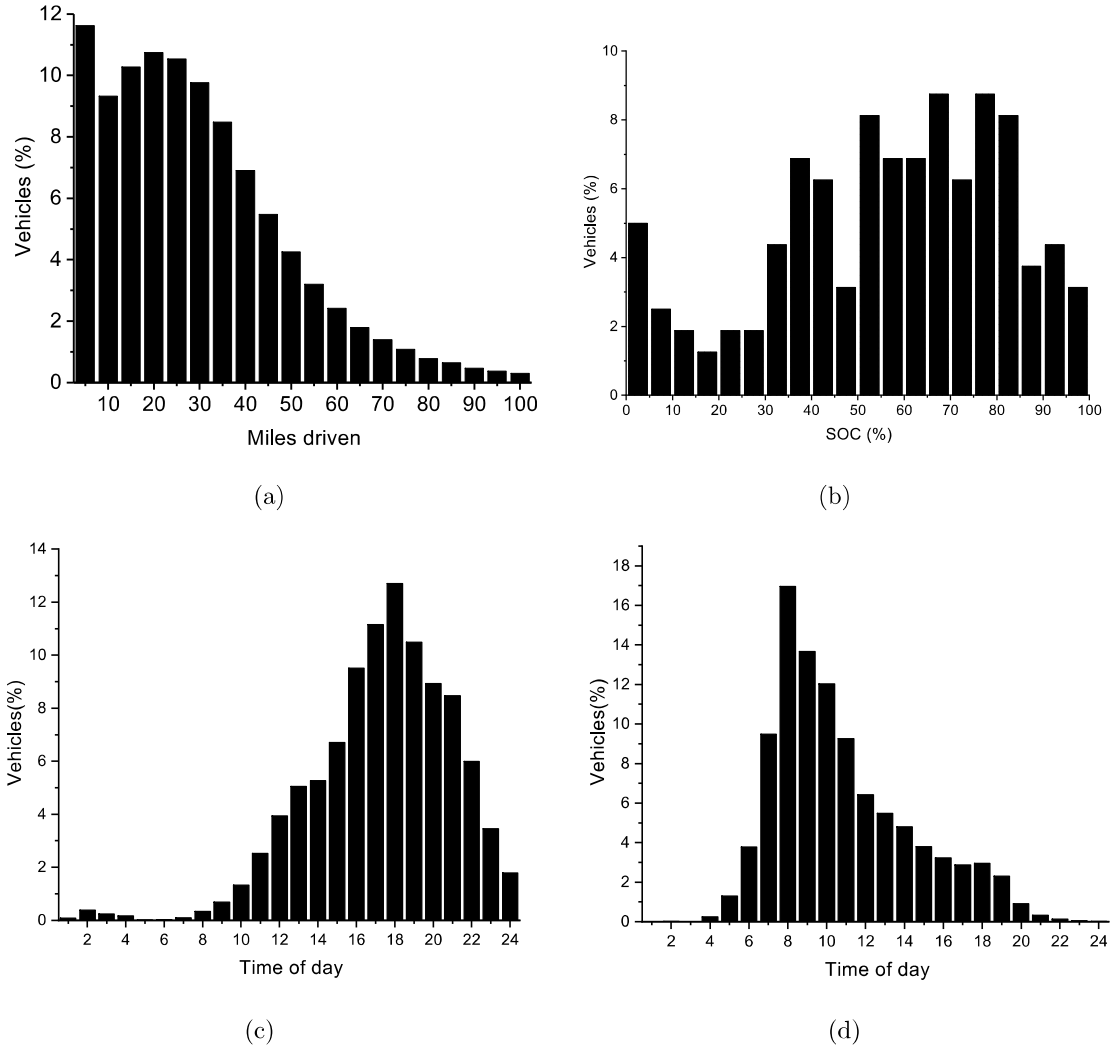

Figure 3.1: (a) Daily miles driven by PHEVs (b) Percentage of vehicles with % SoC level at arrival time (c) Arrival time and (d) departure times

3.4 Methodology

3.4.1 Dantzig–Wolfe decomposition method for decentralized scheduling

For decentralized scheduling of PHEVs, D-BESSs, and other utility assets, a decentralized approach of optimization is employed in the form of Dantzig-Wolfe Decomposition Method (DWDM). DWDM is suitable for linear programs coupled with some constraints. Considering the EV and D-BESS aggregator as optimizing agents, the f_1 given in expression

(3.2), can be reformulated to use DWDM as follows.

$$min\ (C_G + C_{DG} + C_{DGC} + max(C_{EV}) + max(C_{BESS})), \tag{3.34}$$

subject to constraints (3.23)-(3.31). Further, the additional constraints related to load balancing and demand limit (l^{max}) for PHEVs and D-BESSs are defined as follows.

$$P_t^g + \sum_{k=1}^{N_{bus}}(P_t^{dg,k} + \sum_{b=1}^{N_{bess}}(P_t^{d,b,k} - P_t^{c,b,k}) + \sum_{ev=1}^{N_{ev}}(P_t^{d,ev,k} - P_t^{c,ev,k})) = \sum_{k=1}^{N_{bus}} P_t^{L,k}, \tag{3.35}$$

and

$$-l^{max} \leq \sum_{k=1}^{N_{bus}}\sum_{b=1}^{N_{bess}}(P_t^{d,b,k} - P_t^{c,b,k}) + \sum_{k=1}^{N_{bus}}\sum_{ev=1}^{N_{ev}}(P_t^{d,ev,k} - P_t^{c,ev,k}) \leq l^{max}. \tag{3.36}$$

To linearize the problem, the non-linear load flow constraints (3.20)-(3.22) are ignored and only constraints (3.35)-(3.36) are considered as coupling constraints. The master problem and sub-problems for decentralized formulation can be written as follows.

The Master Problem

$$min(C_G + C_{DG} + C_{DGC} + \sum_{w=1}^{W} Z_w^{EV} u_w^{EV} + \sum_{w=1}^{W} Z_w^{BESS} u_w^{BESS}), \tag{3.37}$$

subject to

$$P_t^g + \sum_{k=1}^{N_{bus}} P_t^{dg,k} + \sum_{w=1}^{W}\left(\sum_{k=1}^{N_{bus}}\sum_{ev=1}^{N_{ev}}(P_{w,t}^{d,ev,k} - P_{w,t}^{c,ev,k})u_w^{EV}\right) + \sum_{w=1}^{W}\left(\sum_{k=1}^{N_{bus}}\sum_{b=1}^{N_{bess}}(P_{w,t}^{d,b,k} - P_{w,t}^{c,b,k})u_w^{BESS}\right) = \sum_{k=1}^{N_{bus}} P_t^{L,k} \qquad \boldsymbol{\lambda_t^1}, \tag{3.38}$$

$$-l^{max} \leq \sum_{w=1}^{W}\sum_{k=1}^{N_{bus}}\left(\sum_{ev=1}^{N_{ev}}(P_{w,t}^{d,ev,k} - P_{w,t}^{c,ev,k})u_w^{EV} + \sum_{b=1}^{N_{bess}}(P_{w,t}^{d,b,k} - P_{w,t}^{c,b,k})u_w^{BESS}\right) \leq l^{max} \qquad \boldsymbol{\lambda_t^2, \lambda_t^3}, \tag{3.39}$$

$$\sum_{w=1}^{W} u_w^{EV} = 1 \qquad \boldsymbol{\sigma_{EV}}, \tag{3.40}$$

$$\sum_{w=1}^{W} u_w^{BESS} = 1 \qquad \boldsymbol{\sigma_{BESS}}, \tag{3.41}$$

$$u_w^{BESS}, u_w^{EV} \geq 0, \tag{3.42}$$

where, Z_w^{EV} and Z_w^{BESS} are cost related to PHEVs (-C_{EV}) and BESS (-C_{BESS}) respectively for w^{th} proposal. λ_t^m, σ_{EV}, and σ_{BESS} are dual variable values. The variables u_w^{EV} and u_w^{BESS} are weight factor for w^{th} proposal.

The Sub-Problems

PHEVs and D-BESSs are optimized independently by relaxing the coupling constraints. The sub-problems can be written as follows.

$$min((\rho_t^c + \sum_{m=1}^{3} \lambda_t^m) P_t^{c,ev,k} + (-\rho_t^d - \sum_{m=1}^{3} \lambda_t^m) P_t^{d,ev,k} - \sigma_{EV}), \tag{3.43}$$

subject to constraints (3.24)-(3.28) and (3.31).

$$min((\rho_t^c + \sum_{m=1}^{3} \lambda_t^m) P_t^{c,b,k} + (-\rho_t^d - \sum_{m=1}^{3} \lambda_t^m) P_t^{d,b,k} - \sigma_{BESS}), \tag{3.44}$$

subject to constraints (3.24)-(3.29).

After obtaining load profile of PHEVs and D-BESSs in decentralized manner, it is used as a load for ε-constraints method to minimize four objectives.

3.4.2 The ε-constraint method

During analysis of the distribution system, it is revealed that the term f_4 in the objective function is difficult to handle along with other terms (f_1, f_2, and f_3) in a manner of weighted-sum-objective function. In weighted sum method, optimized results are strongly affected by the scaling of components therein. Therefore, all components should be scaled over a common range, but the value of f_4 varies widely, while the other terms vary over a relatively small range. Hence, it is a difficult task to normalize f_4 as it can be done with other functions. To overcome this problem, ε-constraint method is used. In this method, f_1, f_2, and f_3 are converted into inequality constraints, while the f_4 is treated as an objective function to be minimized. The objective function F can be redefined as

$$Minimize(f_4), \tag{3.45}$$

subject to the following constraints

$$f_1(x) \leq \varepsilon_1,$$

$$f_2(x) \leq \varepsilon_2,$$

$$f_3(x) \leq \varepsilon_3.$$

Here, $\varepsilon_n = max(f_n) - [max(f_n) - min(f_n)] \times \left(\frac{\beta_n}{\alpha - 1}\right)$. The other constraints described in Equations (3.20)-(3.31) are also added to the above set of constraints.

Table 3.2: Tariff of the electrical power

Hour	1	2	3	4	5	6	7	8	9	10	11	12
ρ_t^c(€/kWh)	0.07	0.06	0.06	0.06	0.06	0.06	0.07	0.08	0.09	0.1	0.1	0.1
ρ_t^d(€/kWh)	0.045	0.035	0.035	0.035	0.035	0.035	0.045	0.055	0.065	0.075	0.075	0.075
Hour	13	14	15	16	17	18	19	20	21	22	23	24
ρ_t^c(€/kWh)	0.1	0.1	0.1	0.11	0.12	0.13	0.13	0.15	0.15	0.13	0.11	0.07
ρ_t^d(€/kWh)	0.075	0.075	0.075	0.075	0.08	0.085	0.085	0.09	0.09	0.085	0.075	0.045

3.5 System data and assumptions

The 38-bus distribution network (data given in Appendix II) with three types of loads, i.e. Residential, Commercial and Industrial has been considered for this work. In this distribution system, one main grid and ten different types of curtailable DGs, i.e. PV, wind, and fuel cell are considered. Main grid is connected at bus-1. The optimal locations of the curtailable DGs are determined by solving the optimal location problem minimizing the real power losses. The tariffs for the electricity produced by the grid are given in Table 3.2. The ρ_t^g is considered same as ρ_t^c. The detailed characteristics of DGs, such as type of DGs, energy cost, and optimal locations, are depicted in Table 3.3. The hourly availability of DGs are considered as given in [75]. The DG curtailment cost is considered as 40% of individual DG energy cost.

Table 3.3: Tariff, type, and optimal location of DGs

DGs No.	1	2	3	4	5	6	7	8	9	10
Type	FC	FC	WIND	PV	PV	PV	WIND	WIND	FC	WIND
Bus	2	5	28	8	15	27	3	14	29	30
Price(€/kWh)	0.102	0.095	0.085	0.21	0.178	0.156	0.074	0.136	0.098	0.1

In this study, equally scattered PHEVs and D-BESSs are considered at residential buses. The maximum charging rates of PHEVs and D-BESSs are taken as $4kW/hr$, and $0.8kW/hr$ respectively, whereas the maximum discharging rates are $2.8kW/hr$ and $1.6kW/hr$ for PHEVs battery and D-BESSs respectively. The battery capacity of D-BESS is considered as 4 kWh. The charging and discharging efficiencies are taken as 95% for both PHEVs and D-BESSs. The CO_2 emission rates are given in Table 3.4. The steps of

optimal scheduling are depicted in the flowchart of Figure 3.2.

Table 3.4: CO_2 emission-related parameters

$K_{Co_2-G}(kg/kWh)$	$K_{Co_2-DG}(kg/kWh)$	$K_{Co_2-PHEV}(kg/km)$
1.43	3.07	0.338

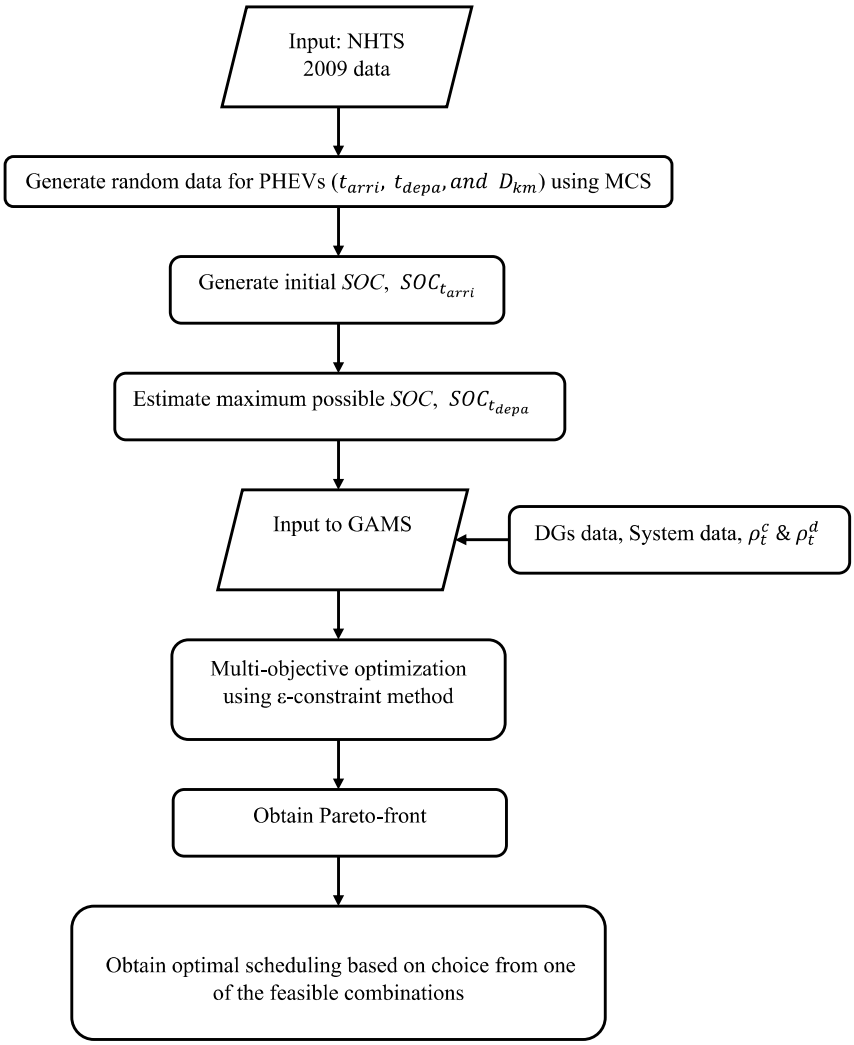

Figure 3.2: Flow chart for optimal scheduling

Following assumptions are made in this work.

- DGs, D-BESSs, and PHEVs are assumed to work at unity power factor.
- Data for the upcoming 24 hours in terms of the driving pattern are available or can appropriately be generated from the available data of the past few days.

- In centralized scheduling, D-BESSs are used by consumers for reliability purposes. These are not operated by profit-based independent retailers for commercial purposes. PHEVs are used by consumers and are equipped with provision of having option for charging/discharging by the utility with some constraints.
- Battery degradation and installation costs are not considered.
- Maximum discharging and charging rates are sufficient to prevent large momentarily release or absorption of energy by consumers for profit maximization.
- Scheduling of PHEVs and D-BESSs are based on forecasted charging and discharging prices. It is assumed that when the schedule is put into operation, the pricing would not be affected by charging/discharging of scheduled D-BESSs and PHEVs.

3.6 Results and discussions

As scheduling of PHEVs (between arrival time and departure time), D-BESSs and DGs is an NLP, GAMS/CONOPT4 solver has been used to minimize the objective function formulated in section 3.2.

The results are discussed in two parts. The first part shows the effectiveness of the proposed objective function, $f_1^{'}$ viz-a-viz f_1 and the second part discusses the effects of optimization on the system under different operating scenarios.

3.6.1 Comparison of objective functions

The outcomes for objective functions f_1 and $f_1^{'}$, in terms of cost to utility, consumer bill, individual consumer benefit, and total discharging power are summarized in Table 3.5. As shown in Table 3.5, f_1 suggests a large number of charging-discharging cycles. From discharging and charging pattern of PHEVs and D-BESSs as shown in Figure 3.3, it is observed that discharging takes place during the period when ρ_t^g is greater than ρ_t^d to minimize f_1, and additional unnecessary charging takes place all over the day to compensate this discharging when f_1 is considered. This happens because there is no effect of charging price in objective function as described in section 3.2.1. It may be noted that the charging and discharging of batteries showing at the same hour in Figure 3.3 correspond to different D-BESSs and PHEVs.

Table 3.5: Comparison of f_1 and $f_1^{'}$

	Cost to Utility	Residential Consumer Bill	Individual Consumer Benefit	Power Discharge	CO_2 Emission	Real Power Losses
Objective f_1	9517.27	2327.108	No	3.8283	107421.1	3.4028
Objective $f_1^{'}$	9629.4	2180.068	Yes	0.32439	106900.8	3.3908

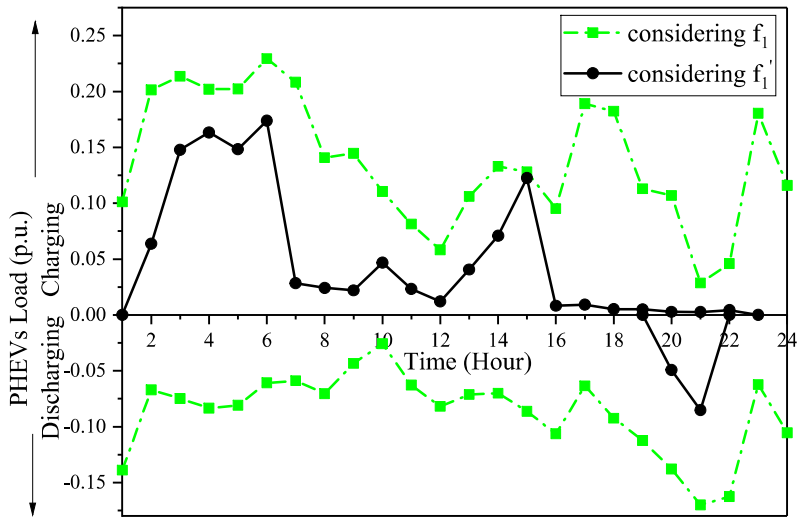

(a)

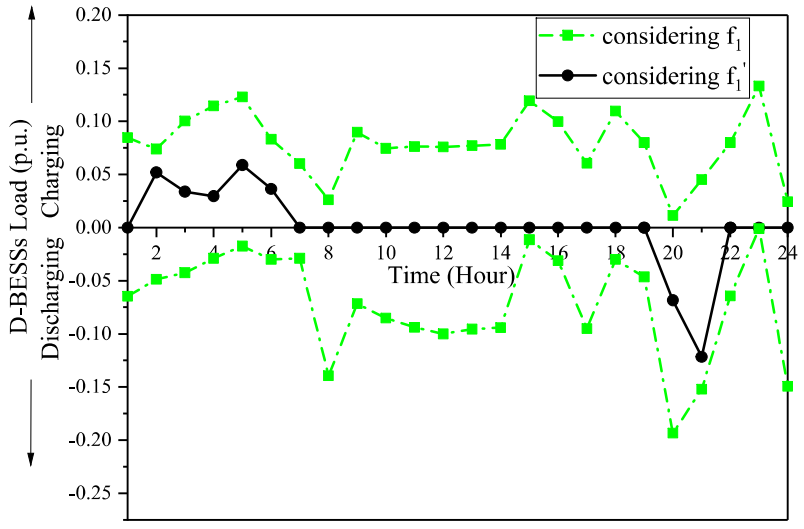

(b)

Figure 3.3: Charging-Discharging profile of (a) PHEVs and (b) D-BESSs. The charging and discharging of batteries showing at same hour, correspond to different D-BESSs and PHEVs.

Real power losses, voltage deviation, and CO_2 emission are also high in case of f_1 as compared to $f_1^{'}$. However, the cost to utility is less when f_1 is considered but it reflects as a high electricity cost for residential consumers. Function $f_1^{'}$ ensures the individual consumer benefit, but it is not observed in f_1. Thus, $f_1^{'}$ is better than f_1 in terms of consumer benefit, and number of charging and discharging cycles. Therefore, it is beneficial to use $f_1^{'}$ for optimization purposes.

3.6.2 Case Studies to demonstrate the system behavior

To demonstrate the system behavior under different scenarios following four cases are considered.

Case-I (Base Case): The base case represents the system under unscheduled charging of PHEVs and there is no penetration of DGs and D-BESSs. In this case, it is assumed that the consumers plugged in PHEVs for charging immediately after the end of their trips and there is no V2G mode. The primary purpose of this case study is to determine the effect of PHEV on the grid, i.e. loading of system, voltage deviations, and power losses.

Case-II: Charging and discharging of PHEVs and D-BESSs are scheduled without DGs (*Case-II(a)*) and with DGs (*Case-II(b)* and *Case-II(c)*) to minimize $f_1^{'}$, f_2, and f_3 using weighted sum method. The weights assigned for $f_1^{'}$, f_2, and f_3 are 0.5, 0.3, and 0.2 respectively. *Case-II(b)* corresponds to a scenario in which the DGs curtailment cost is considered in the objective function whereas *Case-II(c)* corresponds to a scenario in which the DGs curtailment cost is not considered. This case is used to reveal the advantage of scheduled pattern over unscheduled pattern of PHEVs, D-BESSs, and DGs. Case-II(b) and Case-II(c) are used to analyze the effect of penalizing the under-utilization of renewable DGs.

Case-III: In this case, one additional objective f_4 is optimized along with $f_1^{'}$, f_2, and f_3. To overcome the difficulty of including f_4 in weighted sum method (as discussed in section 3.4.2), the ε-constraint method is used to minimize $f_1^{'}$, f_2, f_3, and f_4 simultaneously. This case demonstrates the effect of f_4 on the optimization problem.

Case-IV: In this case, all four objectives are optimized along with consideration of profit maximization of each of the PHEVs and D-BESSs. To achieve this goal, a decentralized approach of optimization is employed for cost objectives of utility, PHEVs,

and D-BESSs as described in section 3.4.1.

The results of the above four cases are discussed below.

Case-I: Figure 3.4 shows the load curve of the system without PHEVs (conventional load) and with PHEVs (Base Case). It is observed that the overall peak load is at noon, and the

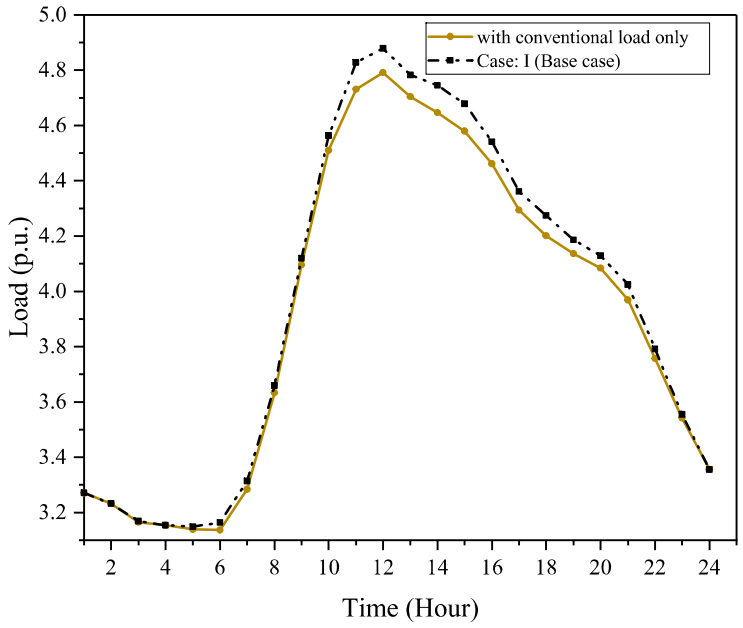

Figure 3.4: Demand curve for main grid

valley occurs at around 4:00 hours. The unscheduled charging profile of PHEVs is shown in Figure 3.5(a). From Figure 3.5(a), it is observed that most of the charging occurs during 11:00 to 18:00 hours. Due to this charging profile, overall peak demand increases from 4.79154 p.u. to 4.87857 p.u. Figure 3.6 shows the bus-wise minimum voltage of the system throughout the day. A minimum voltage of 0.892147 p.u. is observed at bus no. 18. Table 3.6 shows the objective function value F, its components (f_1', f_2, f_3, and f_4), C_G, C_{DG} and other important cost related parameters of the system. From Table 3.6, the PAR can be calculated as 1.2334, which is quite high. The table also indicates high CO_2 emission (134336.967 kg) and real power losses (5.0527 p.u.).

Case-II:

(a) System without DG: Scheduling of PHEVs and D-BESSs- Figure 3.5(a) shows the hourly unscheduled charging profile for the base case scenario (*Case-I*) and the optimally scheduled charging profile (*Case-II*). It is observed that, as a result of scheduling, the charging of PHEVs gets shifted from the peak load period (11:00-18:00 hours) to valley load period (2:00-6:00 hours).

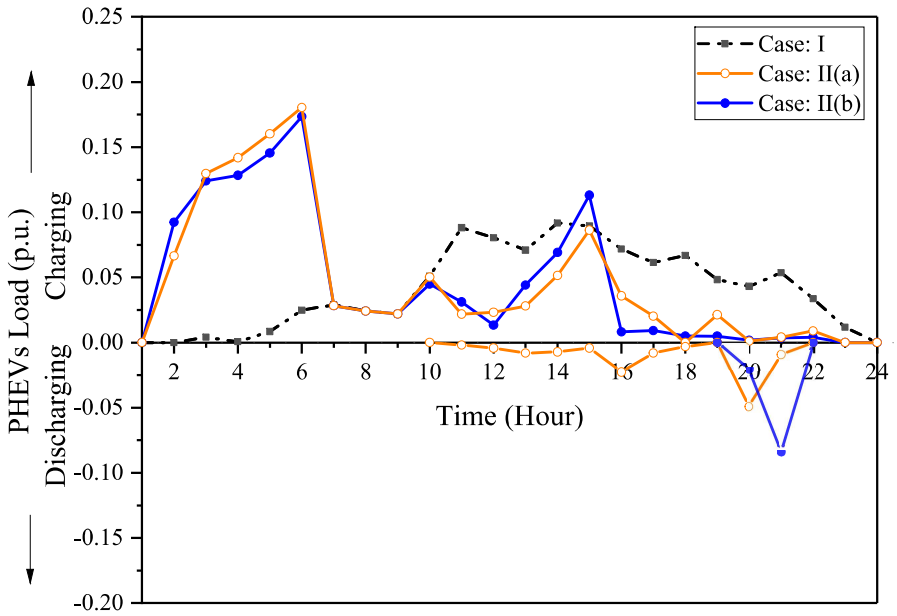

(a)

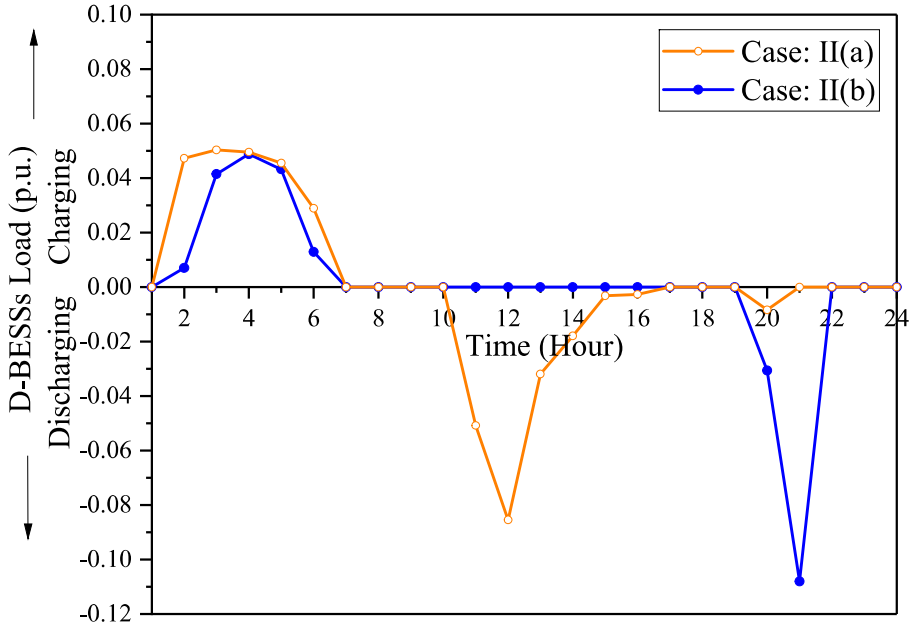

(b)

Figure 3.5: Charging-Discharging profile of (a) PHEVs and (b) D-BESSs

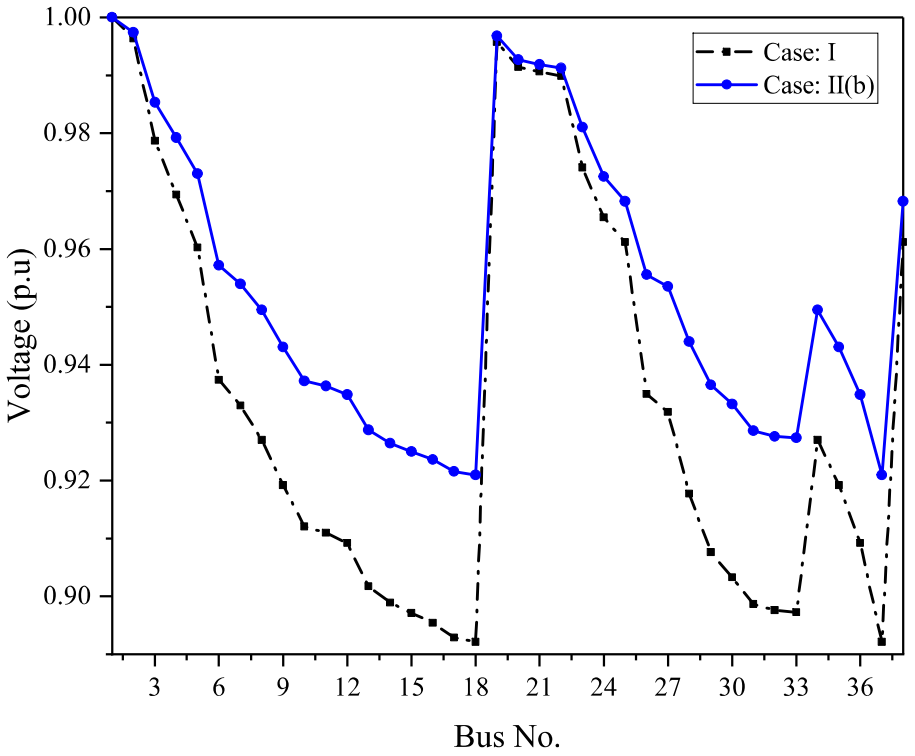

Figure 3.6: Minimum voltage level at 38 buses

Table 3.6: Comparison of *Case-I* and *Case-II*

	Case-I	*Case-II(a)*	*Case-II(b)*	*Case-II(c)*
C_G(p.u. power)	9.3887	9.3383	6.7705	7.1824
C_{DG}(p.u. power)	-	-	2.8951	2.1956
C_{DGC}	-	-	0.0913	0.371
$f_1^{'}$	9.3887	9.3632	9.7788	9.3731
f_2	134336.967	134350.516	101203.9	105001.384
f_3	5.0527	5.0279	3.1575	3.3639
f_4	9.115	6.8769	1.267	0.866
Peak Demand on grid (p.u.)	4.8785	4.7137	3.3017	3.3601
Avg demand on grid (p.u.)	3.9552	3.9556	2.9125	3.0812
Cost to utility(€/day)	9282.9	9266.0	9687.615	9306.9
Cost to residential Consumer(€/day)	2218.5	2184.9	2181.98	2183.7

From Table 3.6, it is observed that when only PHEVs and D-BESSs are scheduled to minimize $f_1^{'}$, f_2, and f_3 then system's peak demand reduces from 4.87857 p.u. to 4.7137 p.u. and cost of system operation reduces from 9282.9 €/day to 9266.0 €/day. It is also observed that peak demand reduces in case of scheduling but the average load increases from 3.9552 p.u. to 3.9556 p.u. The increase in average load is due to the fact that in the latter case, the charging and discharging of d-BESSs and PHEVs are considered. The load increases in *Case-II* as the losses increase due to charging and discharging of PHEVs and D-BESSs. Figure 3.5(b) shows the charging and discharging profiles of D-BESSs over a 24-hour period. It is observed that charging of D-BESSs occurs during valley period (2:00-6:00 hours), at a charging price of 0.06 €/kWh, and D-BESSs discharge power during 11:00-14:00 and 20:00-21:00 hours at a discharging price of 0.075-0.09 €/kWh.

(b) System with DG: Scheduling of PHEVs, D-BESSs and DGs considering DGs curtailment cost- If DGs are also incorporated into the system and scheduled along with PHEVs and D-BESSs then a large portion of total demand can be supplied by the DGs. Figure 3.7 shows the hourly demand curve for the system without DGs (*Case-II(a)*) and for the system with DGs (*Case-II(b)*) after the scheduling of DGs, PHEVs, and D-BESSs. It is observed that the demand on the main substation gets lowered when DGs are employed into the system and scheduled along with PHEVs and D-BESSs.

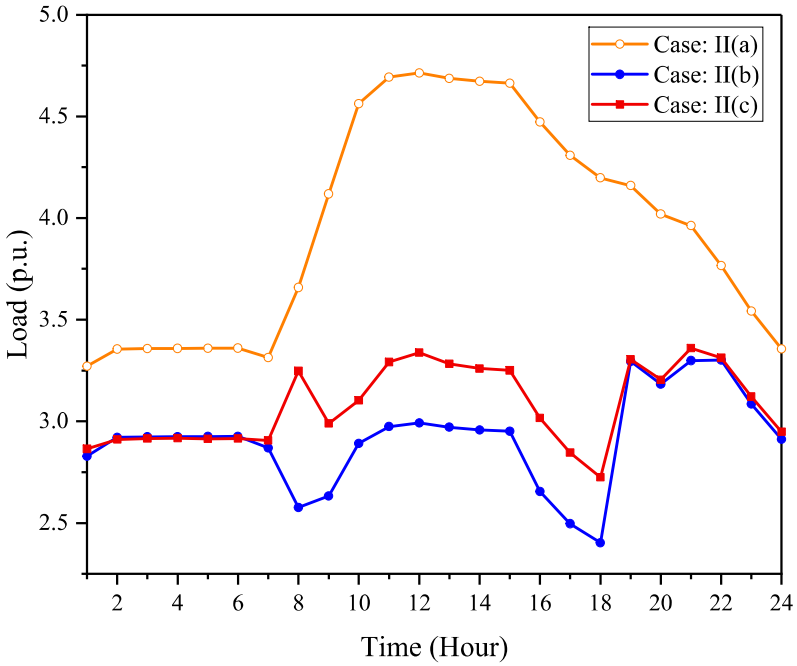

Figure 3.7: Demand curve for main grid for *Case-II*

From Table 3.6, it can be observed that CO_2 emission (f_2) and total real power losses (f_3) are effectively reduced after DGs are employed. However, cost term ($f_1^{'}$) increases from 9.3887 to 9.7788 due to curtailment cost of DGs and high energy price of DGs. Figure 3.6 shows that the minimum voltage level is improved from 0.89214 p.u. to 0.92095 p.u. Figure 3.8 shows the hourly total power supplied by DGs. It can be observed that higher DG power is scheduled during the peak load period as opposed to the valley period. Also, the availability of renewable (especially solar) is higher during the peak hour periods. From Figure 3.9, it is observed that after inclusion of DGs, real power losses are reduced substantially.

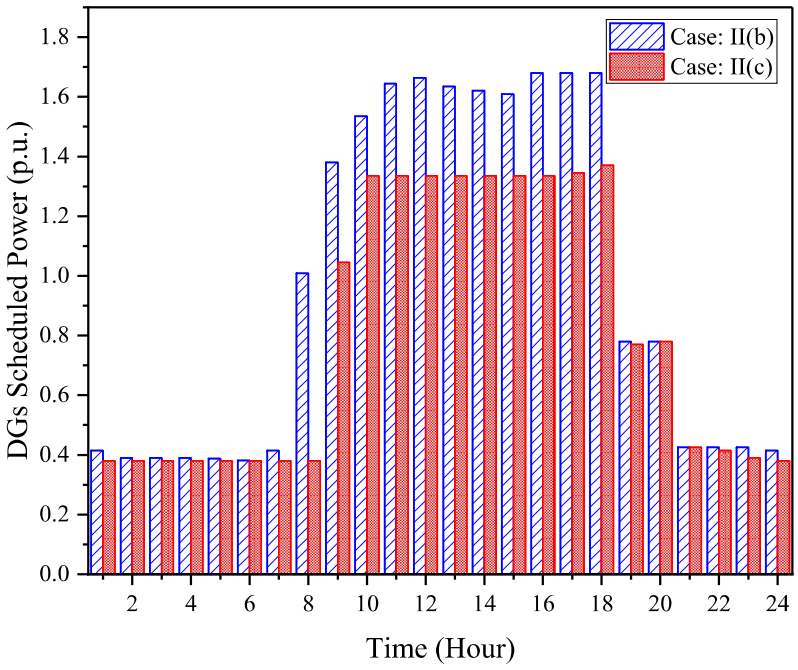

Figure 3.8: DGs Scheduled Power

(c) System with DG: Scheduling of PHEVs, D-BESSs, and DGs without considering DGs curtailment cost- Table 3.6 depicts that without DGs curtailment cost, energy purchase from the grid is preferred than DGs because most of the time, some DGs have high prices as compared to grid. This leads to higher CO_2 emission and real power losses. Figure 3.8 shows that utilization of DGs is low in *Case-II(c)* as compared to *Case-II(b)*. In *Case-II(c)*, value of $f_1^{'}$ is 9.3731 which is lower as compared to *Case-I* and *Case-II(b)*, but f_2 and f_3 are higher as compared to *Case-II(b)*. Therefore, curtailment cost of DGs plays an important role in the utilization of renewable generation.

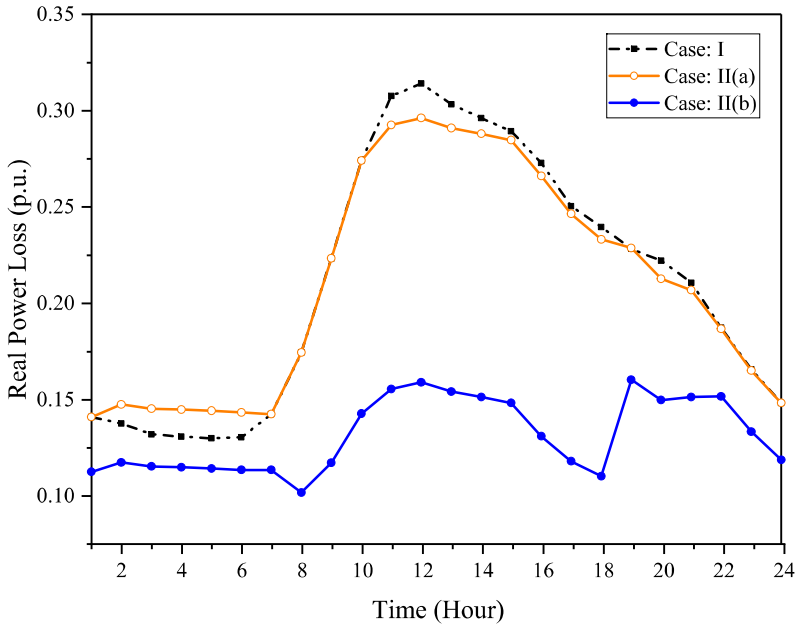

Figure 3.9: Real power losses

Case-III: As discussed in section 3.1, the scaling of the individual objective functions in the weighted sum method strongly affects the results of the optimization. To investigate the range of values of objective functions, a pay-off table is constructed. Such a pay-off table is depicted as Table 3.7.

Table 3.7: Pay-off Table for $f_1^{'}$, f_2, f_3, f_4

	$f_1^{'}$	f_2	f_3	f_4
minimize $f_1^{'}$	**9.7261**	**106900.768**	**3.3908**	0.9357
minimize f_2	**9.8729**	**98310.9080**	**3.1397**	1.6349
minimize f_3	**9.8740**	**100170.3115**	**3.0886**	0.4964
minimize f_4	10.0610	112404.0963	3.6114	5.84×10^{-17}

The first row in Table 3.7 shows that when only objective function $f_1^{'}$ is considered for optimization and the optimal value is 9.7261, then the other functions, f_2, f_3, and f_4 take the values 106900.768, 3.3908 and 0.9357 respectively. Similarly, the other rows of the table depict the values taken by functions when one of them is chosen as the optimization function. The range of values of $f_1^{'}$, f_2, f_3, and f_4 are 9.7261-10.0610, 98310.9080-112404.0963, 3.0886-3.6114, and 5.84×10^{-17}-1.6349 respectively. The pay-off table depicts that there is a large percentage change from maximum to minimum (approx

100%) in a value of f_4 while the other functions change over a small percentage range (3-14%). Hence, it is difficult to normalize f_4 for applying the weighted sum method of constructing the objective function.

Before investigating the effect of additional objective f_4, the ε-constraint method is first applied to $f_1^{'}$, f_2, and f_3 for preparing a case for comparison. For this case, the problem can be defined as minimize $f_1^{'}$ such that f_2 and f_3 are inequality constraints and Pareto Optimal Fronts (POFs) can be obtained as shown in Figure 3.10. From the POFs, it is revealed that most of the solutions are non-inferior. From Figures 3.10(a) and 3.10(b), it is observed that f_2 and f_3 are minimum when $f_1^{'}$ is maximum and vice-versa. From Figure 3.10(c), it is observed that f_2, and f_3 increase monotonically.

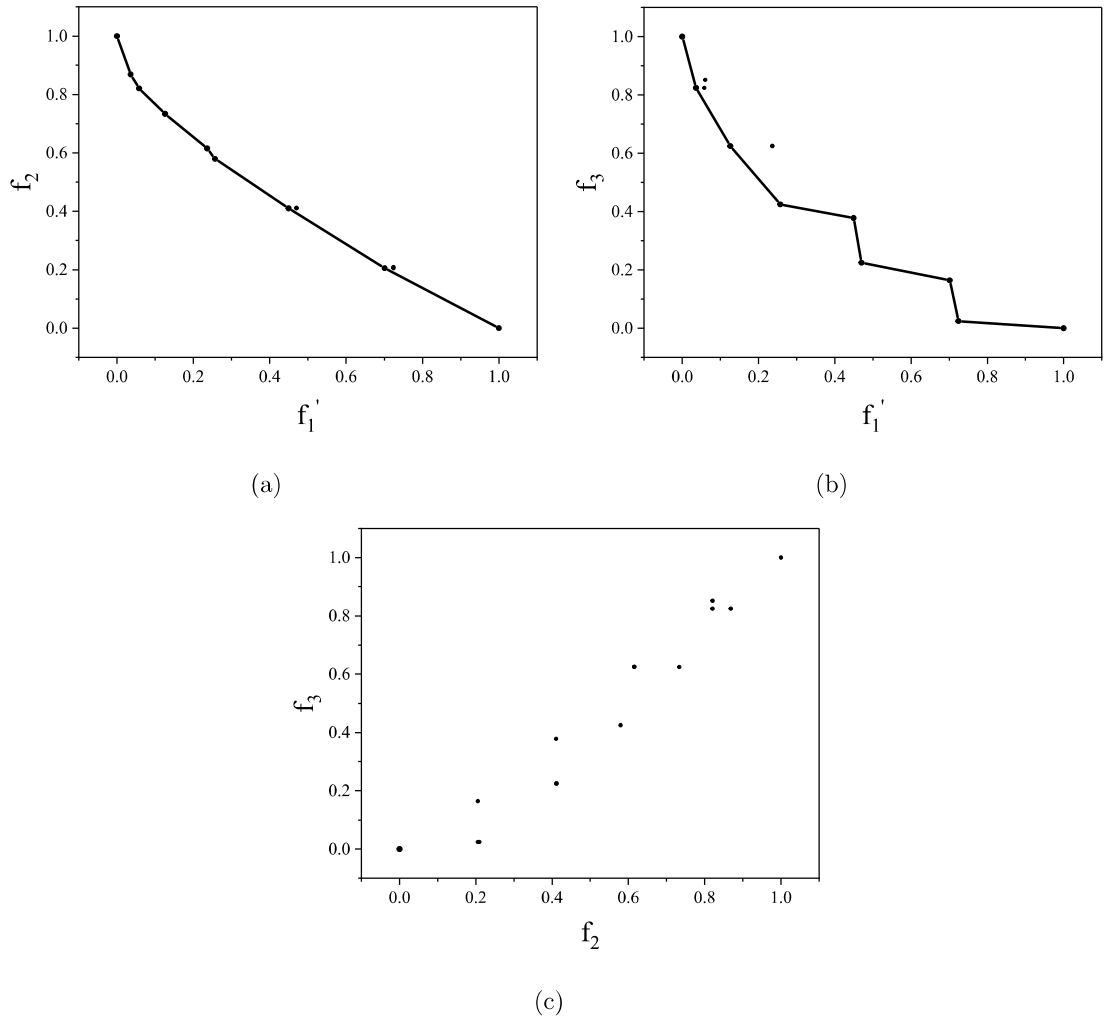

Figure 3.10: Pareto optimal front for different combinations of f_1, f_2, and f_3 if f_4 ignored

Now, the problem can be defined with all four objectives i.e. $f_1^{'}$, f_2, f_3, and f_4 as follows (assuming α=3)

$$min(f_4),$$

subjected to,

$$f_1^{'} \leq (9.8740 - 0.07395\beta_1),$$

$$f_2 \leq (106900.768 - 4294.93\beta_2),$$

$$f_3^{'} \leq (3.3908 - 0.1511\beta_3).$$

Here, β_1, β_2, and β_3 are equal to (0, 1, 2).

Three values of α (3, 4, and 5) are used to generate solutions for obtaining the Pareto Optimal Front (POF) of functions $f_1^{'}$, f_2, f_3, and f_4 for all combinations. The number of possible solutions for the objective functions for α = 3,4, and 5 respectively are 27, 64, and 125, out of which only 13, 34, and 73 are feasible solutions. All 120 feasible solutions are shown in Figures 3.11(a)-3.11(f) for different pairwise combinations of $f_1^{'}$, f_2, f_3, and f_4. Figure 3.11 also depicts the POF consisting of non-inferior solutions. It is observed that a large number of solutions are inferior, if all objective functions ($f_1^{'}$, f_2, f_3, and f_4) are optimized together as compared to the case when f_4 is not considered. Based on one of the feasible combinations of ε-constraint method (α=5 and β_1=β_2=β_3=2) the load curve and scheduled power of PHEVs, D-BESSs, and DGs are shown in Figure 3.12 and Figure 3.13. The outcomes of this case are summarized in Table 3.8. The computation time is 205 seconds for this case on a system having core i7 processor, and 2 GB RAM. From Figure 3.12, it is observed that the demand curve for main grid has very small difference between peak and valley points as compared to the *Case-II(b)* and f_4 reduces from 1.267 to 0.117. After including f_4, PAR is greatly reduced from base load case (1.2334) to 1.044. From Figures 3.13(a) and 3.13(b), it is observed that in *Case-III*, PHEVs and D-BESSs are charged and discharged in a more distributed manner as compared to the *Case- II(b)*. This distributed charging and discharging profiles of PHEVs and D-BESSs is observed due to consideration of f_4 as objective function.

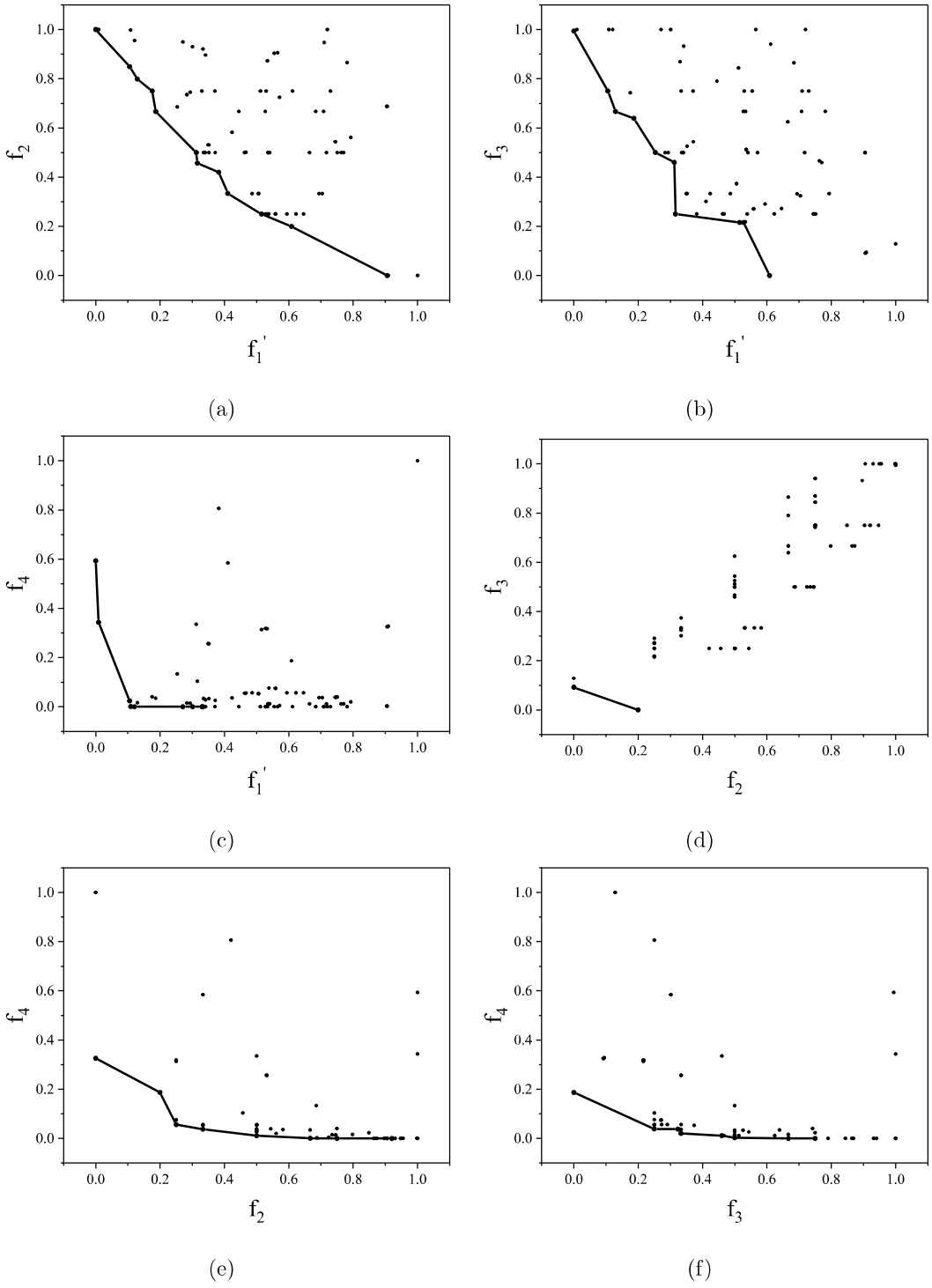

Figure 3.11: Pareto optimal front for different combinations of $f_1^{'}$, f_2, f_3, and f_4

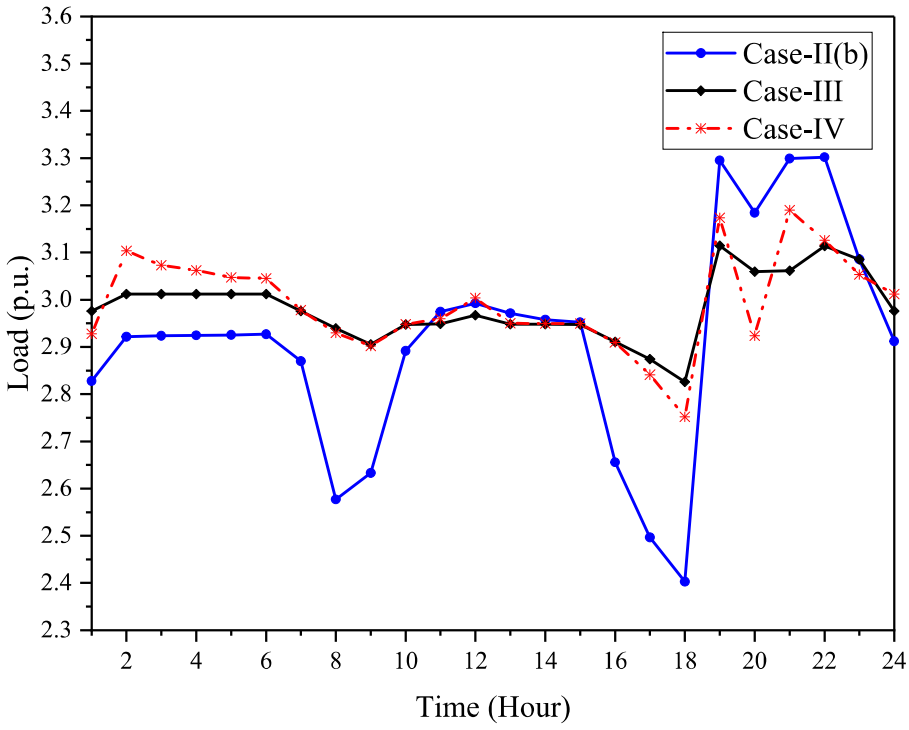

Figure 3.12: Demand curve for main grid for *Case-II(b)*, *Case-III* and *Case-IV* (α=5 and β_1=β_2=β_3=2)

Table 3.8: Outcomes of *Case-III* ans *Case-IV*

	Case-III	*Case-IV*
C_G(p.u. power)	6.8955	6.9054
C_{DG}(p.u. power)	2.6196	2.5927
$f_1^{'}$	9.8000	9.8017
f_2	102605.9	102751.4
f_3	3.2300	3.2516
f_4	0.117	0.240
Peak Demand on grid (p.u.)	3.1145	3.1896
Avg demand on grid (p.u.)	2.9827	2.9920
PAR	1.044	1.067
Cost to utility(€/day)	9651.4	9659.37
Cost to residential Consumer(€/day)	2177.83	2167.90

In *Case- II(b)*, it is preferred to charge PHEVs and D-BESSs during low charging-

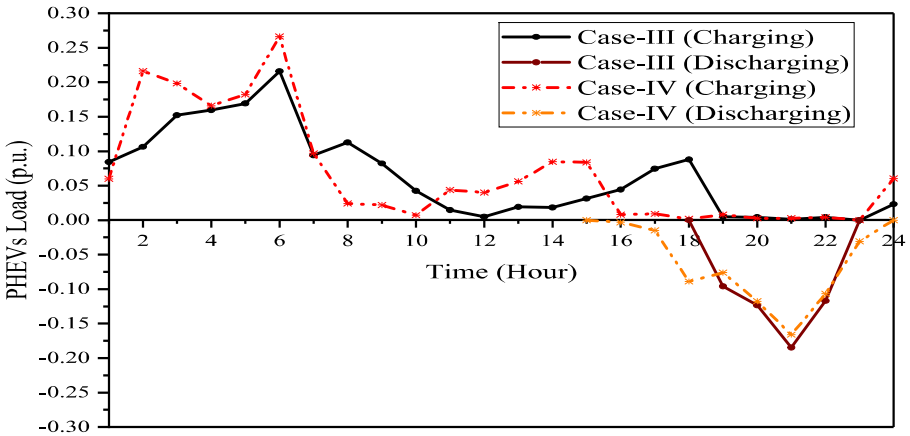

(a)

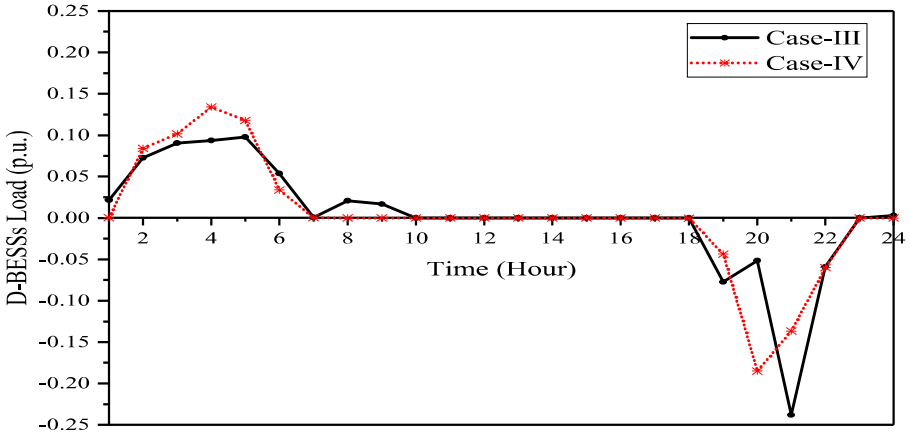

(b)

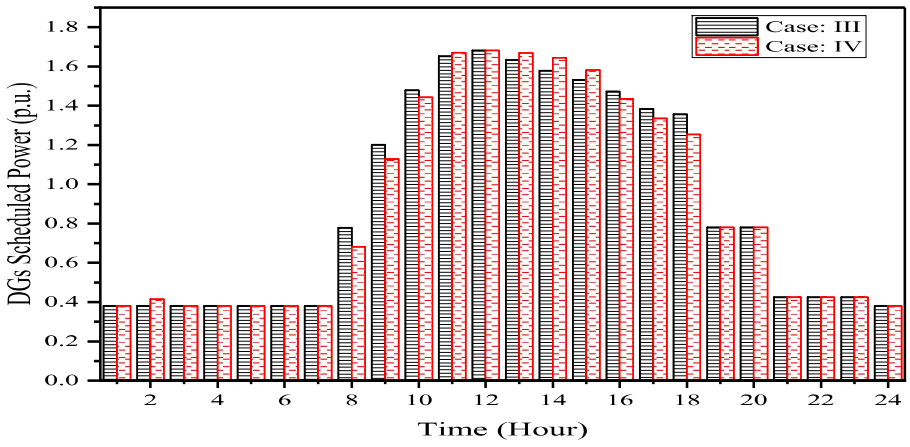

(c)

Figure 3.13: Scheduled Power of (a) PHEVs, (b) D-BESSs, and (c) DGs for *Case-III* and *Case-IV* (α=5 and β_1=β_2=β_3=2)

price period as much as possible to reduce $f_1^{'}$. Function f_2 is independent of time, as it only depends on how much power is generated from conventional power sources and fuel cells. So overall objective function F ($f_1^{'}$, f_2, f_3) has low value if charging occurs during low charging-price period and discharging occurs during high charging-price period. However, in *Case- III*, both $f_1^{'}$ and f_4 are optimized simultaneously. It is observed that in both, *Case-II(b)* and *Case-II(c)*, the load flattening (f_4) is high when f_4 is not a component in the objective function. *Case-III* corresponds to a situation when f_4 corresponding to load flattening is also considered in the objective function. The f_4 is reduced notably when it is considered as a part of the objective function.

It is observed that some portions of PHEVs and D-BESSs charging shift from 2:00-6:00 hours to 7:00-9:00 hours and discharging of PHEVs and D-BESSs gets distributed between 19:00-22:00 hours. The reason behind this shifting is that the DGs provide less power during 1:00-6:00 and 19:00-24:00 hours period, as shown in Figure 3.13(c). Hence, it is necessary to make charging and discharging profile of PHEVs and D-BESSs more distributed to minimize f_4.

Case-IV: Figure 3.12 depicts the comparison of load curves for the *Case-II(b)*, *Case-III*, and *Case-IV* when l^{max} (limit imposed on net demand of PHEVs and D-BESSs) equals to 0.3 p.u. It is observed that the peak load for *Case-II(b)* is the highest, whereas for *Case-III* the peak load is lowest. Figure 3.13(a) and 3.13(b) show that when decentralized approach for scheduling of PHEVs and D-BESSs are employed, the charging is concentrated during 2:00-6:00 hours due to low charging price. The charging is more pronounced in *Case-IV*, than that of *Case-III*. Therefore, the load profile has a higher peak value in *Case-IV* as compared to *Case-III* during 2:00 to 6:00 hours. Changes in different parameters in *Case-IV* as compared to *Case-III* are depicted in Table 3.8. In *Case-IV*, the cost to utility increases from 9651.4 to 9659.37 €/day and cost to residential consumers decreases from 2177.83 to 2167.90 €/day. The cost to residential consumers decreases up to a limit as l^{max} increases, but induces a high peak in the load curve.

3.7 Summary

An ϵ-constraint method is used to obtain 24-hour scheduling of DGs, BESSs/D-BESSs, and PHEVs in V2G & G2V mode. Different case studies show that effective schedul-

ing can be obtained with significant load flattening if the proposed approach is adopted, which keeps the cost, CO_2 emission, and losses at lower levels. The detailed analysis of proposed cost-function for charging and discharging was made. The analysis shows that re-formulated cost function effectively provides scheduling solutions eliminating unnecessary charging and discharging of BESSs/D-BESSs and PHEVs. Case studies carried in this chapter and detailed analysis of results show that peak load reduction, system cost, CO_2 emissions and losses are dealt more effectively with the proposed method and the proposed cost function. The analysis through pay-off table shows that the multi-objective problem of load flattening and cost cannot be dealt with effectively as a weighted sum objective. The proposed method can assist Local Distribution Companies (LDC) in assessing cost minimization, CO_2 emission minimization, real power losses minimization and load flattening simultaneously.